Journal of Hazardous Materials 196 (2011) 318–326

Contents lists available at SciVerse ScienceDirect

Journal of Hazardous Materials

journal homepage: www.elsevier.com/locate/jhazmat

Co^{2+}-exchange mechanism of birnessite and its application for the removal of Pb^{2+} and As(III)

Hui Yin, Fan Liu, Xionghan Feng, Mingming Liu, Wenfeng Tan, Guohong Qiu*

Key Laboratory of Subtropical Agricultural Resources and Environment, Ministry of Agriculture, College of Resources and Environment, Huazhong Agricultural University, Wuhan 430070, PR China

ARTICLE INFO

Article history:
Received 28 May 2011
Received in revised form 30 August 2011
Accepted 8 September 2011
Available online 14 September 2011

Keywords:
Birnessite
Ion exchange
Octahedron vacancy
Cobalt oxidation
Lead adsorption
Arsenite oxidation

ABSTRACT

Co-containing birnessites were obtained by ion exchange at different initial concentrations of Co^{2+}. Ion exchange of Co^{2+} had little effect on birnessite crystal structure and micromorphology, but resulted in an increase in specific surface areas from 19.26 to 33.35 $m^2\,g^{-1}$, and a decrease in both crystallinity and manganese average oxidation state. It was due to that Mn(IV) in the layer structure was reduced to Mn(III) during the oxidation process of Co^{2+} to Co(III). The hydroxyl groups on the surface of Co-containing birnessites gradually decreased with an increase of Co/Mn molar ratio owing to the occupance of Co(III) into vacancies and the location of large amounts of $Co^{2+/3+}$ and $Mn^{2+/3+}$ above/below the vacant sites. This greatly accounted for the monotonous reduction in Pb^{2+} adsorption capacity, from 2538 mmol kg^{-1} for the unmodified birnessite to 1500 mmol kg^{-1} for the Co^{2+} ion-exchanged birnessite with a Co/Mn molar ratio of 0.16. The amount of As(III) oxidized by birnessite was enhanced after ion exchange, but the apparent initial reaction rate was greatly decreased. The present work demonstrates that Co^{2+} ion exchange has great influence on the adsorption and oxidation behavior of inorganic toxic metal ions by birnessite in water envrionments.

1. Introduction

Birnessite is a kind of ubiquitous hydrous-layered manganese oxide (phyllomanganate) in geological environments [1]. Usually occurring as fine-grained particles, it exhibits high reactivity and is widely involved in a series of geochemical processes, particularly plays a pivotal role in the fate of heavy metal(loids) (Pb^{2+}, Cd^{2+}, As(III), Cr(III) and so on) and other pollutants in contaminated soil and water systems, due to mixed valences, large surface area and low point of zero charge [2–9].

Cobalt is one of the trace elements enriched in deep-sea manganese nodules and crusts [10]. It is also found that manganese minerals present in soils contain relatively large amount of Co [11]. Manganese oxides remarkably affect the geochemistry behavior of Co likely due to the electron transfer between adsorbed Co^{2+} and high-valence Mn [12–17]. A direct evidence for the oxidation of Co^{2+} to Co^{3+} on the surface of manganese oxides was first reported by Murray and Dillard [18] using XPS. Previous literatures have suggested that surface-adsorbed Co^{2+} on birnessite could be oxidized by certain Mn(IV) in the vicinity of vacancies [18,19]. During the reactive transport of Co(II)$EDTA^{2-}$ by pyrolusite (β-MnO_2), Mn(IV) was reduced to Mn(III) rather than Mn(II) to form a stable trivalent manganese solid (α-Mn_2O_3), which passivated the surface after an initial reaction period and ultimately limited the yield of Co(III)$EDTA^-$ [20]. However, X-ray powder diffraction and polarized EXAFS spectroscopy were combined to determine the Co-sorbed birnessite and indicated that Mn^{3+} is the more likely electron sink for the oxidation of Co^{2+} [21]. These results indicated that, during the adsorption and oxidation of Co^{2+} by manganese oxides, the electron sink, whether the Mn(IV) or the Mn(III), is mostly likely dependent on the manganese oxide structures, surface chemical characteristics and reaction conditions. However, the mechanism of Co^{2+} oxidation by acid birnessite is not clear yet.

Furthermore, as for the first transition-metal series, Co(III), Mn(III), and Mn(IV) have similar ionic radius and charges, and all can stably exist in layered structures composed of edge-sharing octahedra [22]. However, the electronegativity of cobalt is different from that of manganese in similar crystallographic structures, and the Co^{3+}/Co^{2+} redox conjugate pair has a higher standard reduction potential than those of $MnO_2/Mn^{3+}/Mn^{2+}$ [23]. Thus, incorporation of cobalt may have some influence on the crystal structure, morphology, manganese average oxidation state (Mn AOS), and hydroxyl content of birnessite, subsequently on the removal of toxic metal(loids) from wastewater. The adsorption, oxidation, and ion exchange are common characteristics of elemental geochemistry. Our previous work demonstrated that the adsorption performance and removal capacity for Pb^{2+} and As(III) from aquatic systems by acid birnessite could be improved remarkably

* Corresponding author. Tel.: +86 27 87280271; fax: +86 27 87280271.
E-mail address: qiugh@mail.hzau.edu.cn (G. Qiu).

0304-3894/$ – see front matter © 2011 Elsevier B.V. All rights reserved.
doi:10.1016/j.jhazmat.2011.09.027

after doping with cobalt during the synthesis process [24]. In this paper, Co-containing birnessites obtained by ion exchange with Co^{2+} at different concentrations were synthesized, characterized, and their adsorption and oxidation performance towards Pb^{2+} and As(III) were investigated, respectively. The ion-exchange process and underlying mechanism was further studied.

2. Materials and methods

2.1. Sample preparation

Acid birnessite was prepared according to McKenzie's method [25]. Co^{2+} adsorption was conducted by adding $Co(NO_3)_2$ solution to a birnessite suspension (1.67 g L^{-1}) with pH 5 at 25 °C. The pH of the mixtures was maintained by adding 0.1 mol L^{-1} HNO_3 and NaOH solution. The Co concentration in solution was adjusted to obtain Co/Mn molar ratios, such as 0, 0.02, 0.05, 0.10, and 0.20. After allowing 24 h for equilibration, the samples were filtered, rinsed, and dried at 40 °C for several days, and then ground and sieved (100 mesh). The prepared Co-containing birnessite samples were designated as HB, HC2, HC5, HC10, and HC20 according to the initial Co coverages, respectively.

2.2. Sample characterization

All samples were characterized by powder XRD, FTIR, SEM, N_2 adsorption, and chemical analysis. XRD analyses were carried out on a Bruker D8 Advance diffractometer equipped with a Lynx-Eye detector using Ni-filtered Cu Kα radiation (λ = 0.15418 nm). The diffractometer was operated at a tube voltage of 40 kV and a tube current of 40 mA with 1.2 s counting time per 0.02° 2θ step. FTIR analyses were conducted on a Bruker Equinox 55 model spectrophotometer using KBr pellets with a spectral range of 4000–400 cm^{-1}. The final spectrum was the average of 64 scans at a nominal resolution of 4 cm^{-1}. The crystallite morphologies of the samples were probed by scanning electron microscopy using a JSM-6390LV microscope after being coated with a gold evaporated film. The specific surface area was obtained by nitrogen adsorption using an Autosorb-1 standard physical adsorption analyzer (Quantachrome Autosorb-1). The samples were degassed at 110 °C for 3 h under vacuum prior to adsorption measurement.

The chemical compositions of the samples were determined using atomic absorption spectrometry (AAS, Varian AAS 240FS) and flame spectrometry (Sherwood Model 410). 0.1000 g of sample was dissolved in 25 mL solution of 0.25 mol L^{-1} $NH_2OH{\cdot}HCl$ and 1 mol L^{-1} H_2SO_4. The Mn AOS was obtained by a titration method: a mass of 0.2000 g sample was completely reduced to Mn^{2+} in 5 mL of 0.5000 mol L^{-1} $H_2C_2O_4$ and 10 mL of 1 mol L^{-1} H_2SO_4. Excess $C_2O_4^{2-}$ was determined by back-titration using a $KMnO_4$ standard solution at 75 °C [26].

2.3. XPS analysis

X-ray photoelectron spectra were collected using a VG Multilab2000 X-ray photoelectron spectrometer with an Al Kα X-ray source (1486 eV) and a base pressure of 3×10^{-9} Torr in the analytical chamber. The scans were recorded using the large area mode. The survey scans were collected using a fixed pass energy of 100 eV and an energy step size of 1.0 eV, whereas the narrow scans had a pass energy of 25 eV and an energy step size of 0.1 eV. The spectra were analyzed using the Avantage software. The Shirley-type background was subtracted before deconvolution and fitting. A ratio of 30:70 of the Lorentzian: Gaussian mix-sum function was used for all the fittings.

A broad asymmetric peak was observed for C (1s) (Fig. S1). Three peaks were used to fit C (1s) spectra (Table S1 and Fig. S1) corresponding to alkyl type carbon (C–C, C–H), alcohol (C–OH) and/or ester (C–O–C) functionalities, and C=O/ O–C=O, respectively. All samples have been charge corrected to give the adventitious C (1s) spectral component (C–C, C–H) a binding energy of 284.80 eV. This process has an associated error of ±0.1–0.2 eV [27,28].

2.4. Pb^{2+} adsorption experiments

Pb^{2+} adsorption experiments were performed and details on the experimental procedure are reported in our previous work [24]. A solid/solution ratio of 1.67 g L^{-1}, initial Pb^{2+} concentration ranges from 0 to10 mmol L^{-1}, and a constant supporting electrolyte concentration ($NaNO_3$, I_c = 0.1 mol L^{-1}) were used. The mixtures were shaken at a rate of 250 r min^{-1} for 24 h at 25 °C, and the pH of the reaction system was maintained at 5.00 using a pH-stat technique in the process. The metal ions (Pb^{2+}, Mn^{2+}, Co^{2+}, and K^+) in solution were analyzed by AAS and flame spectrometry.

2.5. As(III) oxidation experiments

The procedure of As(III) oxidation was also the same as that documented in reference [24]. A solid/solution ratio of 0.5 g L^{-1}, 0.08 mmol L^{-1} of initial As(III) concentration, and a constant supporting electrolyte concentration ($NaNO_3$, I_c = 0.1 mol L^{-1}) were used. The reaction was carried out at pH 7 with stirring at 25 °C. As(V) was measured using the colorimetric method [29]. Release amount of Co^{2+}, Mn^{2+} and K^+ was monitored by AAS and flame spectrometry.

3. Results and discussion

3.1. Characterization

3.1.1. Crystal structure of the Co-containing birnessites

Fig. 1 shows the powder XRD patterns of the obtained samples. The patterns could be indexed corresponding to Hexagonal, R-3m (JCPDS 86-0666). Birnessite was characterized by four detectable peaks: 0.723, 0.361, 0.244, and 0.142 nm. Peaks at 0.723 nm and 0.361 nm were both symmetrical, belonging to (0 0 *l*) reflections, whereas the other two at higher angles were broad. The 0.244 nm peak is convoluted by (1 0 1) and (0 1 2) reflections while the 0.142-nm one is convoluted by (1 1 0), (1 1 3) and (10, 13) reflections (JCPDS 86-0666). The intensity of the 0.361-nm peak was higher than that of the 0.244-nm peak, which suggested that the diffracting crystallites contained more layers stacked coherently along the *c* axis than that of "acid birnessite" reported by Villalobos et al. [30,31].

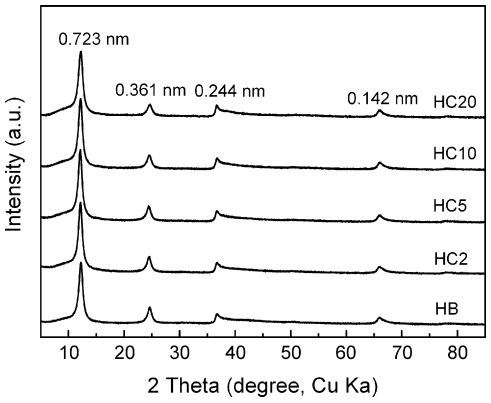

Fig. 1. Powder XRD patterns of birnessite and Co-containing birnessites.

Table 1
Physicochemical properties of Co-containing birnessites.

Sample	Element content (%)			Co/Mn ratio	Mn AOS	SSA ($m^2\ g^{-1}$)
	Mn	Co	K			
HB	52.74	0	8.36	0	3.78	19.26
HC2	50.43	1.16	6.65	0.02	3.68	19.14
HC5	49.57	2.77	5.61	0.05	3.65	18.43
HC10	48.25	5.90	4.39	0.11	3.59	28.70
HC20	46.96	7.88	3.00	0.16	3.56	33.35

Co-containing birnessites exhibited the same XRD characteristics as the original sample. There were four peaks with similar symmetry and relative intensity. As the initial molar ratios of Co/Mn increased, no extra peak was detected, suggesting that the import of cobalt ions into the lamellar birnessite did not affect the crystal structure, and no second phase was introduced. However, the peak intensity of Co-containing birnessites slightly decreased, and their FWHM slightly increased, indicating a decrease in particle size and crystallinity. This was further confirmed by the monotonous decrease in the relative intensity of the 0.361-nm peak to the 0.244-nm peak.

3.1.2. Elemental analyses and Mn AOS

Table 1 shows the content of Co, Mn, and K in birnessite before and after adsorption reaction. The initial Co/Mn molar ratio was controlled as 0.02, 0.05, 0.10, and 0.20 in the adsorption experiment, and it was changed to be 0.02, 0.05, 0.11, and 0.16 in birnessite, respectively. When the initial concentration was low, all Co^{2+} ions were adsorbed. However, when the initial molar ratio of Co/Mn increased to 0.20, only 80% Co^{2+} ions could be retained. The final molar ratio of Co/Mn was lower than that obtained by ion exchange of HBir with Co^{2+} by Manceau et al. [21]. This was ascribed to that vacant sites (16.7%) in HBir were higher than those in acid birnessite (12%) [31]. The content of potassium was reduced by 20.5%, 32.9%, 47.5%, and 64.1%, respectively, compared to HB, due to the replacement of quite a relatively large amount of K^+ by Co^{2+}.

The Mn AOS of Co-free birnessite was 3.78, confirming the mixed valence states of Mn in the form of Mn^{3+} and Mn^{4+} with Mn^{4+} being the predominant species. The Mn AOS gradually decreased with an increase in cobalt content (Table 1).

3.1.3. FTIR analysis

Fig. 2 presents the FTIR spectra of Co-containing birnessites. Five well-resolved peaks were observed at 3412, 1619, 920, 506 and 436 cm^{-1}. The first two bands were ascribed to the stretching and bending vibrations of molecular H_2O [32]. Vibrations of Mn–O bond in the structure of birnessite were reflected at 506 and 436 cm^{-1}, which resembled the natural analogs [33,34]. Due to

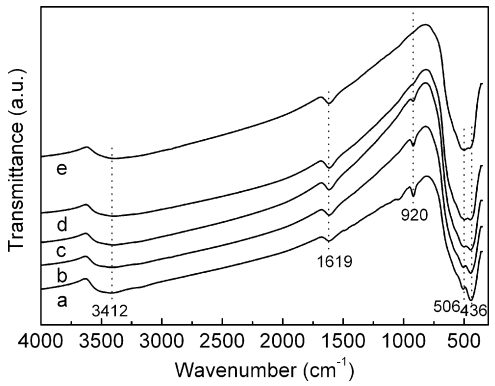

Fig. 2. FTIR spectra of Co-containing birnessites: (a) HB, (b) HC2, (c) HC5, (d) HC10, and (e) HC20.

that the absorption band at 423 cm^{-1} could indicate the crystalline order [34], the decrease of the adsorption band intensity suggested the lower degree of crystallinity for Co-containing composites.

It was noteworthy that the intensity of the adsorption peak at 920 cm^{-1} gradually decreased with an increase in Co content. As [MnO_6] octahedral layer in birnessite containing vacancies was similar to that of [AlO_6] layer in the structure of dioctahedral clay minerals. As for the latter, 2/3 octahedra were occupied by cations. These cations were coordinated to OH groups, which were parallel to the (0 0 1) planes and pointing to vacant sites. If two Al^{3+} cations were located there, vibration frequencies of Al–Al–OH were 911–917 cm^{-1} [35]. For the similar electronegativity of Mn^{3+} (HS, $\chi = 1.675$), Mn^{4+} (HS, $\chi = 1.923$) in the [MnO_6] octahedron of birnessite with Al^{3+} ($\chi = 1.515$), and coordination radius of Mn^{3+} ($r = 0.785$ Å), Mn^{4+} ($r = 0.670$ Å) with Al^{3+} ($r = 0.675$ Å), it could be inferred that the vibration of Mn–Mn–OH in the vicinity of vacancy was close to 911–917 cm^{-1} [36–38]. Therefore, the decrease in the peak intensity at 920 cm^{-1} was possibly due to that the content of hydroxyl groups around vacancies gradually decreased after Co^{2+} ion exchange reaction.

3.1.4. Micromorphology

Fig. 3 shows the SEM images of birnessite formed by three-dimensional (3D) hierarchical microspheres consisting of two-dimensional (2D) nanoplates. The radius of the 3D microspheres was approximately 200 nm in diameter. Cobalt induction had no obvious effect on the micromorphologies of the products but slightly reduced the particle dimensions.

3.1.5. Specific surface area

The surface areas of the samples are listed in Table 1. The specific surface area of HB was 19.26 $m^2\ g^{-1}$, which was similar to that reported by Mckenzie [13]. After ion-exchange reaction, the surface area values of HC2, HC5, HC10, and HC20 were determined to be 19.14, 18.43, 28.70, and 33.35 $m^2\ g^{-1}$, respectively. As indicated by XRD patterns, FTIR, and SEM images, the crystallinity of Co-containing samples gradually decreased. The specific surface area increased with a decrease in crystallinity of birnessite.

3.2. Surface analysis using XPS

X-ray photoelectron spectroscopy is recently being used to investigate the abundance and chemical state of elements in the uppermost few atomic layers of solid surfaces. Fig. S2 shows the broad scans for all samples. The peak at a BE of 780 eV was the photoelectron line of cobalt, and its intensity gradually increased with an increase in Co content. The photoelectron line of K (2p) was at the left of C (1s). Its relative intensity greatly decreased for Co-containing birnessites compared to HB, suggesting a lower abundance of potassium in samples after Co^{2+} ion exchange, which coincided with the results of the chemical analysis.

In order to determine the chemical states of Mn, Co and O on the surface of Co-containing samples, narrow scans were also performed. To obtain the relative quantity of Mn^{2+}, Mn^{3+}, and Mn^{4+} on birnessite surface, the Mn ($2p_{3/2}$) spectrum was fitted [28,39]. Table S2, Fig. 4 and Table 2 show the parameters used and the fitting results, respectively. The content of Mn^{4+} gradually decreased from 79.83% in HB to 66.90% in HC20 while Mn^{3+} increased from 13.72% to 23.70%, and Mn^{2+} content slightly increased. According to the fitting results, the calculated Mn AOS were 3.73, 3.71, 3.68, 3.62, and 3.58 for HB, HC2, HC5, HC10 and HC20, respectively. These results agreed well with the titration data (Table 1).

Narrow scans for Co (2p) are plotted in Fig. 5. The measured BE values for Co ($2p_{1/2}$) and Co ($2p_{3/2}$) were 795 and 780 eV, respectively, similar to those of Co(III)OOH reported by Crowther et al. [19]. Furthermore, the Co($2p_{1/2}$)–Co($2p_{3/2}$) splittings were identical

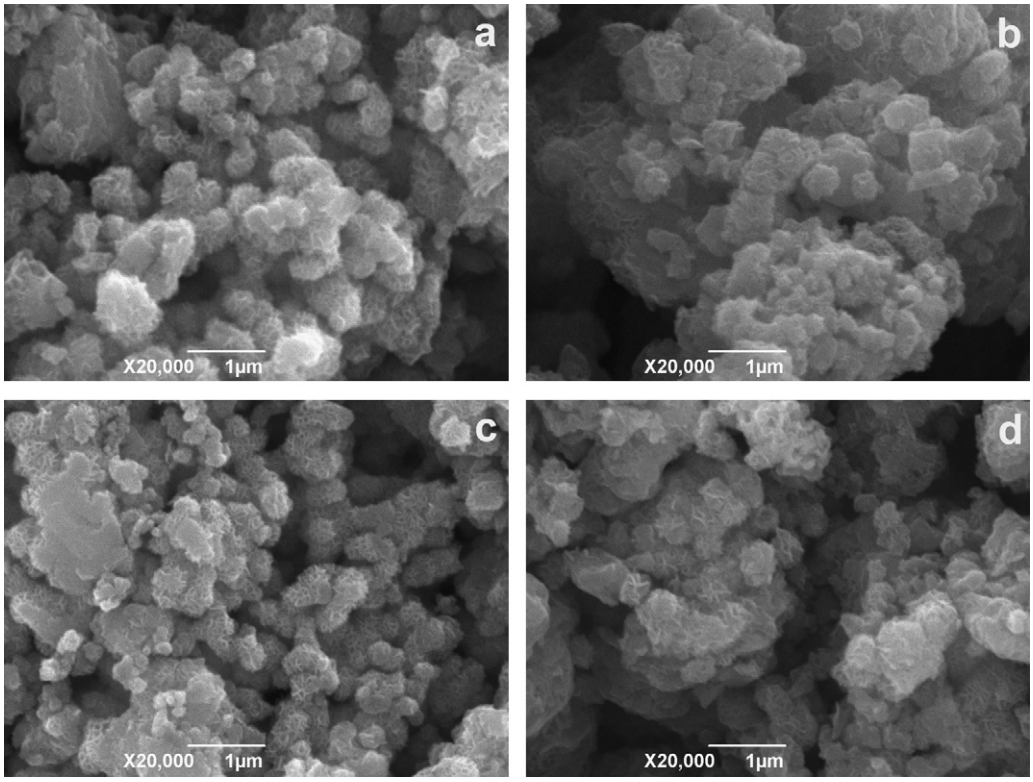

Fig. 3. SEM of birnessites before and after ion exchange with Co^{2+} at different concentrations: (a) HB, (b) HC2, (c) HC5, and (d) HC20.

at 15.0 eV(±0.20 eV) which was a characteristic of the spectrum of Co(III) compounds [19]. These results suggested that Co(III) mainly existed in the samples.

After being adsorbed on the surface of birnessite, Co^{2+} was oxidized to Co(III) by high valence Mn in the structure. As illustrated by elemental analysis and multi-component fitting of Mn ($2p_{3/2}$) spectra of Co^{2+} ion-exchanging hexagonal birnessites, the Mn AOS are generally lower than +4, indicating the coexistence of Mn^{4+}, Mn^{3+}, and Mn^{2+} in the structure. Both Mn^{4+} and Mn^{3+} can accept electron from Co^{2+}, but acid birnessite with hexagonal layer symmetry has the most intricate and polytropic structure characteristics. It consists of edge-sharing [Mn(IV)O_6] octahedra, [Mn(III)O_6] octahedra, and vacancies. Large quantities of cations, such as H^+, K^+, and $Mn^{2+/3+}$, exist in the interlayer space of adjacent layers to balance the high negative permanent structural charge originated from the substitution of Mn(IV) by Mn(III) and vacancies within the octahedral sheet [31,40–42]. It is difficult to investigate the oxidation mechanism of Co^{2+} due to the complex structure of birnessite.

The element composition in HB changed after ion exchange with Co^{2+}. Variations (Δ) in the quantity of Mn(IV), Mn(III), Mn^{2+}, and Co(III) were calculated and summarized in Table 3 based on the results of chemical composition (Table 1) and XPS (Table 2). As for HC20, the content of Mn(IV) was reduced by 2353 mmol kg^{-1} Mn, whereas Mn(III) and Mn(II) were increased by 1817 and 535 mmol kg^{-1}, respectively. The amount of Co(III) imported was 2847 mmol kg^{-1}. Given that Mn^{2+} was adsorbed almost totally on the surface of birnessite as Mn^{2+} was not detected during the ion exchange process, $\Delta(Mn^{2+})$ should be equal to $\Delta(Co^{3+})$ if the layer and/or interlayer Mn(III) was the oxidant as proposed by Manceau et al. [21]. However, $\Delta(Mn^{2+})$ was only about 1/5 of $\Delta(Co^{3+})$. HC2, HC5 and HC10 all generally abided to this rule. In the present work, the Mn(IV) was most likely the electron acceptor.

Two possible pathways for the Co^{2+} oxidation by Mn(IV) were proposed in this study. In the first pathway, two moles of Co^{2+} reacted with one mole of Mn(IV), producing one mole of Mn^{2+} and two moles of Co(III) as Eq. (1):

$$Mn(IV) + 2Co^{2+} \rightarrow Mn^{2+} + 2Co(III) \quad (1)$$

As for the above equation, $\Delta(Mn^{2+}) = -\Delta(Mn^{4+}) = (1/2)\Delta(Co^{3+})$, and $\Delta(Mn^{3+})$ should be no more than zero (for disproportionation). The other pathway involved one mole of Mn(IV) participating in the oxidation of one mole of Co^{2+} to Co(III), and Mn(IV) was reduced to Mn(III):

$$Mn(IV) + Co^{2+} \rightarrow Mn(III) + Co(III) \quad (2)$$

Table 2
Near-surface compositions of Mn and O species derived from fittings of Mn ($2p_{3/2}$) and O (1s) spectra.

Sample	Mn (at.%)			O (at.%)		
	Mn^{4+}	Mn^{3+}	Mn^{2+}	O^{2-}	OH^-	H_2O
HB	79.83	13.72	6.46	54.78	22.45	22.77
HC2	77.87	15.32	6.81	60.26	22.03	17.71
HC5	75.71	16.90	7.39	56.98	21.42	21.60
HC10	70.76	20.76	8.48	59.02	18.88	22.10
HC20	66.90	23.70	9.40	57.74	17.00	25.26

Table 3
Variances in the content of Mn(IV), Mn(III), Mn^{2+} and Co(III) in Co-containing birnessites.

Sample	$\Delta(Mn^{4+})$[a]	$\Delta(Mn^{3+})$	$\Delta(Mn^{2+})$	$\Delta(Co^{3+})$
HC2	−357	291	64	390
HC5	−750	579	169	948
HC10	−1651	1281	368	2075
HC20	−2353	1817	535	2847

[a] "−" means that the content of Mn^{4+} decreased.

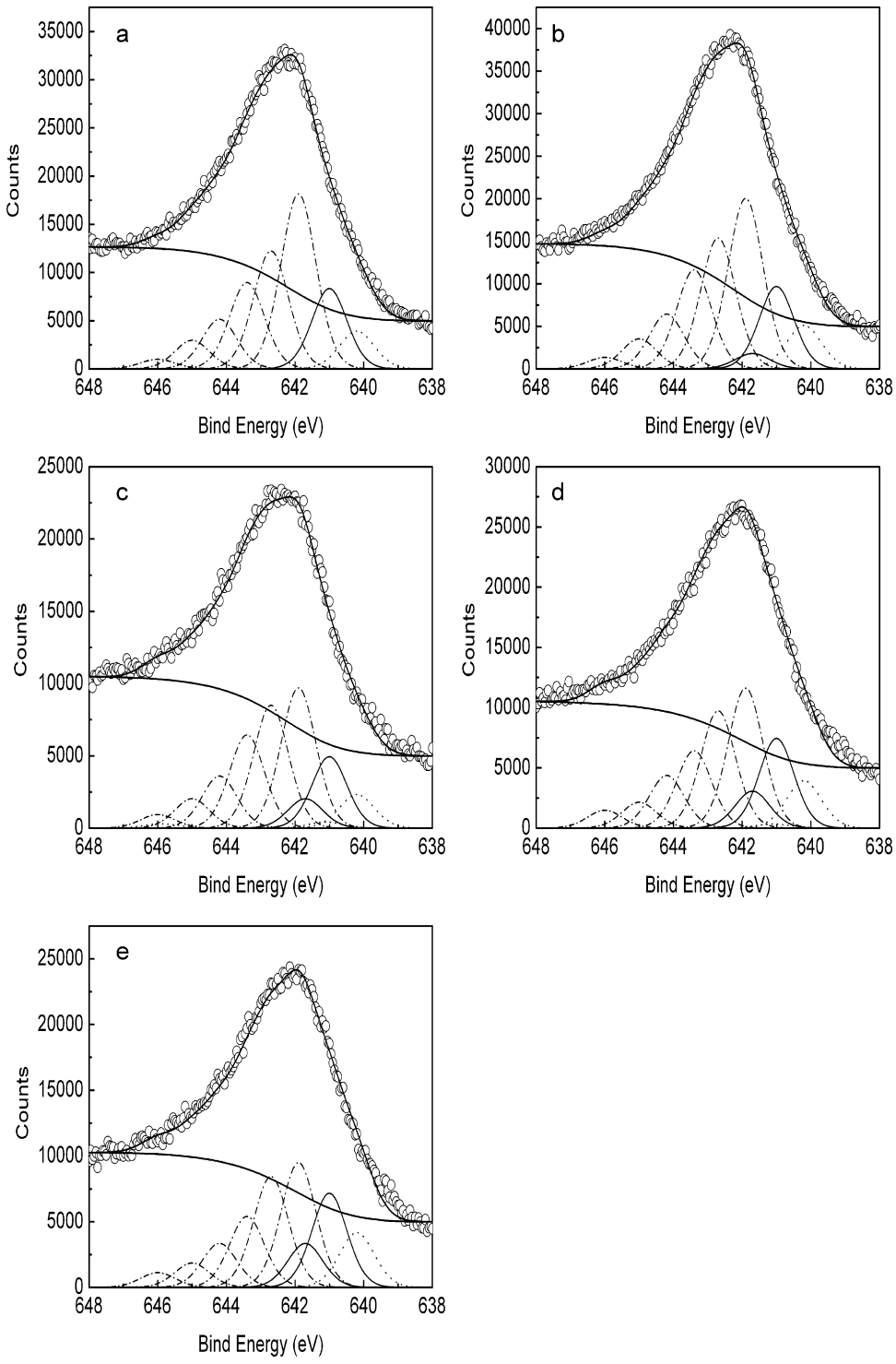

Fig. 4. Mn ($2p_{3/2}$) spectra of Co-containing birnessites: (a) HB, (b) HC2, (c) HC5, (d) HC10, and (e) HC20 (The upper circles represent the observed data, and the thick, solid curve is the best fit of the data. The dash-dot curves represent Mn(IV) multiplet peaks, while the thin, solid curves are Mn(III) and the dotted lines are Mn(II).).

If Eq. (2) occurred, $\Delta(Mn^{3+}) = -\Delta(Mn^{4+}) = \Delta(Co^{3+})$ should be correct. However, Mn(III) are unstable and disproportionate as follows [43]:

$$2Mn(III) \rightarrow Mn(IV) + Mn^{2+} \quad (3)$$

Therefore, the change trend of various species should increase in the order: $\Delta(Mn^{2+}) < \Delta(Mn^{3+}) < -\Delta(Mn^{4+}) < \Delta(Co^{3+})$, in agreement with the results as listed in Table 3. Consequently, Mn(III) was the primary reduction product of Mn(IV).

The O (1s) spectra of as-prepared birnessites had main characteristic peaks at 529.94, 529.93, 529.88, 529.61 and 529.75 eV. The electronegativity (χ) values of Mn^{3+} (HS, $\chi = 1.675$) and Co^{3+} (LS, $\chi = 1.791$) in the $[Mn(Co)O_6]$ octahedron of birnessites were lower than that of Mn^{4+} (HS, $\chi = 1.923$) [36,37]. Larger amounts of Mn^{3+} and Co^{3+} in the layer led to an increase in the ionic bond character of the Mn(Co)–O bond. Therefore, the electron cloud density of cores of O^{2-} and OH^- increased, and their BEs shifted to the lower.

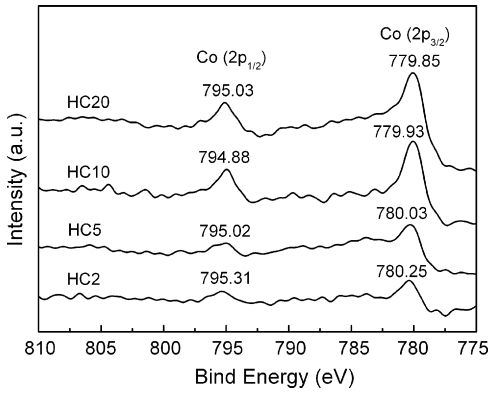

Fig. 5. Co (2p) spectra of Co-containing samples.

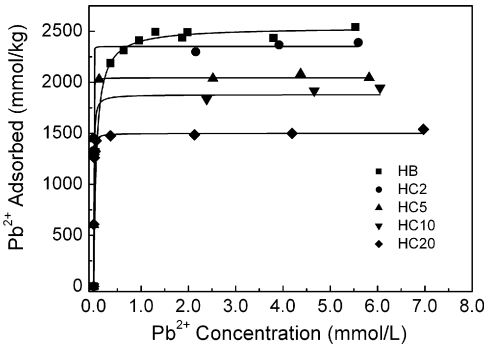

Fig. 6. Isothermal curves of Pb^{2+} uptake by Co-containing birnessites.

Lattice oxygen (O^{2-}), hydroxide oxygen (OH^-), and oxygen in molecular water (physisorbed, chemisorbed, and structural H_2O and water in poor electrical contact with the mineral surface) [44] were the three oxygen species in birnessite materials corresponding to the main peak, the broad shoulder, and the pronounced tail, respectively. The peak parameters used in fitting O (1s) spectra are listed in Table S3 and the corresponding results are presented in Fig. S3 and Table 2, respectively. The content of hydroxide group gradually decreased with an increase of cobalt content, which was consistent with the FTIR results.

3.3. Adsorption of Pb^{2+} by Co-containing birnessites

Lead is one of the widespread contaminant in water systems. Its concentration in many industrial water bodies was reported to be as high as 200–500 mg L^{-1}. This concentration is very high in relation to the current water quality standard of 0.05–0.1 mg L^{-1} [45,46]. Consequently, it is essential to reduce the lead levels in wastewater before it was discharged.

In order to investigate the effect of Co^{2+} ion exchange on the Pb^{2+} adsorption behavior by birnessite, as-prepared composites were used for removal of Pb^{2+} in laboratory artificial waste water at the concentration level of 0–10 mmol L^{-1} at 25 °C.

The adsorption of Pb^{2+} on birnessites conformed to the L-type isotherm [47]. The removal efficiency of Pb^{2+} increased sharply when the equilibrium concentration of Pb^{2+} was increased from the lowest value, indicating a high affinity isotherm with strong preference for solid phase partitioning in these systems. Then the removal efficiency increased slightly, and last tended to remain stable and approached a maximum as the equilibrium Pb^{2+} concentration increased (Fig. 6).

The Langmuir equation was shown as Eq. (4):

$$Q = \frac{A_{max}KC}{1 + KC} \quad (4)$$

where Q is the amount of Pb^{2+} adsorbed (mmol kg^{-1} mineral), A_{max} the maximum adsorption capacity (mmol kg^{-1}), C the equilibrium concentration of the adsorbate (mmol L^{-1}), and K a constant related to the adsorption energy as function of temperature and adsorption enthalpy [48]. The adsorption capacities are listed in Table 4. HB had a capacity of 2538 mmol Pb^{2+} per kilogram birnessite. Co^{2+} ion exchange lessened the removal of Pb^{2+} from solution by birnessite. The maximum capacity of Pb^{2+} removed by HC2, HC5, HC10 and HC20 were 2352, 2045, 1879 and 1500 mmol kg^{-1}, respectively. These as-obtained birnessites exhibited more effective adsorbability for Pb^{2+} in aqueous solution than other reports, such as single manganese oxides [5], and manganese oxide coated sand, zeolite and bentonite [3,49,50].

Birnessite has the highest affinity for Pb^{2+} among various heavy metal ions [5]. Pb(II) forms strong inner-sphere surface complexes mainly at two sites on hexagonal birnessite nanoparticles: triple corner-sharing (TCS) surface complexes and triple edge-sharing (TES) surface complexes on vacancies, and double corner-sharing (DCS) and double edge-sharing (DES) complexes on lateral edge surfaces [51]. Regardless of whatever Pb(II) complexes formed, the content of vacancies in birnessite structure positively determined the adsorption capacity for Pb^{2+} [52]. But some other literatures reported that, the external edge surface played a key role in Pb^{2+} adsorption. A positive linear relationship between BET surface area and maximum Pb^{2+} capacity had been established [53]. Nevertheless, the surface areas of birnessites treated with different concentrations of Mn^{2+} greatly increased from 9.84 m^2 g^{-1} to 67.0 m^2 g^{-1}, but their Pb^{2+} adsorption capacity gradually decreased [52]. Therefore, the total Pb^{2+} adsorption capacity was determined not only by the content of vacant sites and the surface areas, but also by their relative abundance. In the Pb(II) uptake experiments of biogenic manganese oxides, the surface areas of the minerals were much high for their finite crystal size, and the contribution for Pb uptake by external sites was higher than the internal sites. However, as for the Co-containing birnessites here, although the surface areas of Co-containing composites was increased from 19.26 to 33.35 m^2 g^{-1} with an increase in cobalt content (Table 1), Pb^{2+} adsorption capacity gradually decreased (Fig. 6; Table 4). This decrease was probably attributed to the decrease of the content of vacant sites. As demonstrated by Manceau et al. [21], when Co^{2+} was adsorbed on vacancies and then oxidized to Co^{3+}, most of the Co^{3+} directly incorporated into the vacant sites, and

Table 4
Langmuir parameters for the adsorption of Pb^{2+} and maximum concentrations of Mn^{2+}, Co^{2+}, H^+, K^+ released.

Sample	Parameters			Ions released (mmol kg^{-1})			
	A_{max} (mmol kg^{-1})	K	R^2	Co^{2+}	Mn^{2+}	H^+	K^+
HB	2538	17.7	0.998	0	0	2778	1283
HC2	2352	4484	0.999	18.9	0.5	2629	978
HC5	2045	1222	0.995	34.6	0.5	2297	730
HC10	1879	165.3	0.987	78.9	9.1	2304	546
HC20	1500	349.6	0.998	174.9	34.7	2199	372

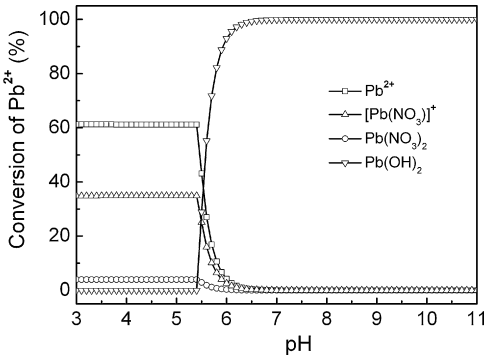

Fig. 7. Speciation of lead(II) as a function of pH. [Pb] = 10 mmol L^{-1} in 0.1 mol L^{-1} $NaNO_3$ (calculated using ECOSAT4.9 [54]).

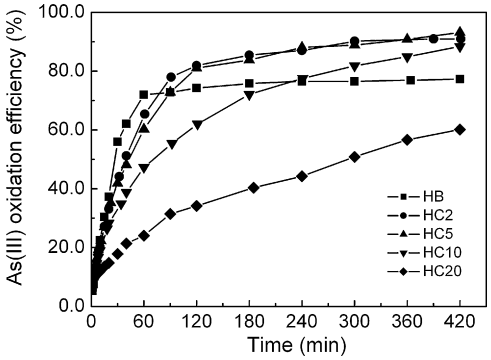

Fig. 8. Kinetics curves of As(III) oxidation by Co-containing birnessites.

partial $Co^{3+/2+}$ was located above or below vacancies, resulting in the decrease of the number of vacant sites and the content of hydroxyl groups. The decrease of vacant sites loudly accounted for the decrease of Pb^{2+} adsorption capacity. Although the location of $Co^{3+/2+}$ on the vacancies did not affect the amount of vacant sites, but these cations would compete with Pb(II) species for binding sites. Therefore, the maximum lead adsorption capacity of Co^{2+}-exchange birnessites was greatly reduced. This was different from the case of Pb^{2+} adsorption by Co-doped birnessites. The enhanced Pb^{2+} removal of Co-doped birnessites compared with the undoped one was attributed to the gain of negative charge of the octahedral layer by the substitution of layer Mn(IV) by Co(III) and the induction of vacancies in the structure by the insertion of Co(III) because of the heterogeneity between the exotic ion and $Mn^{4+/3+}$ [24].

During Pb^{2+} adsorption, Mn^{2+}, Co^{2+}, H^+, and K^+ were simultaneously released into the solution in the order: $H^+ > K^+ > Co^{2+} > Mn^{2+}$ (Table 4). This implied that the negative charge of birnessite layer was mainly balanced by H^+ and K^+. Mn^{2+} was not detected during Pb^{2+} adsorption by HB, indicating the presence of small amounts of $Mn^{2+/3+}$ in the interlayer, which was consistent with the XPS results. The release amount of H^+ and K^+ was positively related to the Pb^{2+} adsorbing capacity, however, that of Co^{2+} and Mn^{2+} increased with the increase of cobalt content. With an increase in cobalt content, more Mn^{2+} ions were released into the solution. These low valence Mn ions were formed from the reduction of $Mn^{3+/4+}$ by Co^{2+}. About 9.6%, 7.4%, 7.9% and 13.1% of the total cobalt in HC2, HC5, HC10 and HC20 was released, respectively. It indicated that there might be some Co^{2+}, existing in the interlayer or on the surface of birnessite besides Co^{3+} when the initial Co^{2+} concentration was high [21]. The Co^{2+} can be replaced by Pb^{2+} during the adsorption. Furthermore, the Co^{3+} in the interlayer might also be driven by Pb^{2+} into the solution coupled with redox reactions, but the underlying mechanisms are not clear yet.

The aqueous speciation of Pb^{2+} is shown in Fig. 7 as a function of pH in the range of 3–11 (calculated using ECOSAT4.9 [54]). When pH was below 5.4, Pb^{2+} and $[Pb(NO_3)]^+$ were the main species. As it increased to 5.4, the formation of $Pb(OH)_2(s)$ began to limit the concentrations of aqueous species. At ~pH 5.5, $Pb(OH)_2(s)$ was the major form present in the system. When pH was above ~6.5, Pb(II) occurred predominantly as $Pb(OH)_2(s)$. At pH 5.0, the species of Pb(II) in the adsorption systems existed as Pb^{2+} (61.21%), $[Pb(NO_3)]^+$ (34.84%), and $Pb(NO_3)_2$ (3.95%).

According to the charge conservation law in the process of ion exchange, two moles of H^+ and/or K^+ or a mole of divalent cation (Me^{2+}) would be released after the adsorption of one mole of Pb^{2+} whereas adsorption of $[Pb(NO_3)]^+$ would drive only one mole of H^+ or K^+ or 1/2 mol of Me^{2+} away from the surface of birnessite. This was confirmed by the algebraic relationship of the amounts of Pb(II) adsorbed and the release of ions as follows:

$$n(Pb(II)) \times (0.6121 \times 2 + 0.3484) \approx n(H^+) + n(K^+) + (n(Mn^{2+}) + n(Co^{2+})) \times 2$$

where n denotes the amount of adsorbed/released ions, and was listed in Table 4.

3.4. Effects of Co^{2+}-exchange on the oxidation of As(III)

Arsenic contamination is an issue of great concern. Depending on its source, arsenic concentrations in natural waters may range up to several hundred milligrams per liter. Due to its acute toxicity to humans, a maximum contaminant level (MCL) should be less than 10 μg L^{-1} for arsenic in drinking water [55].

Manganese oxides are reactive oxidants for the transformation of As(III) to As(V) under natural conditions. As-prepared birnessites were used to study the oxidative transformation of sodium arsenite at the interface of minerals and water. Arsenite oxidation first occurred quickly and the reaction rate then decreased to keep a balance after 1–2 h. HC2 and HC5 had the same shape as that of HB. However, in the case of HC10 and HC20, the oxidation amount of As(III) gradually increased as the reaction progressed (Fig. 8).

An apparent oxidation capacity of As(III) to As(V) was calculated to evaluate the oxidation ability of birnessite, due to the fact that adsorption and fixation of As(III) and As(V) occurred simultaneously during the oxidation process [8]. The calculated apparent oxidation capacity of As(III) by HB is 77.3% at equilibrium. After reaction for 7 h, the conversion of As(III) to As(V) by HC2, HC5, HC10 and HC20, were 91.0%, 93.2%, 88.4% and 60.2%, respectively. High oxidation ability towards As(III) was ascribed to the participation of Co(III) in the reaction, since the standard reduction potential for Co^{3+}/Co^{2+} (E° = 1.92 V) is higher than the MnO_2/Mn^{2+} (E° = 1.224 V) and Mn^{3+}/Mn^{2+} (E° = 1.5415 V) half reactions [23]. This was already confirmed in our previous work using XPS analysis [24].

The relationship of As(III) concentration with time was analyzed by fitting a first-order rate equation to the 0–0.33 h portions of all the five systems (Fig. 9). The apparent reaction rate constants (k_{obs}) of HB, HC2, HC5, HC10, and HC20 were calculated to be 0.0226, 0.0175, 0.0161, 0.0123, and 0.0035 min^{-1}, respectively. The higher initial reaction rate of As(III) oxidation for HB than for Co-containing ones can be ascribed to several reasons. Firstly, in Co-containing birnessites, oxygen atoms bound to Co^{3+} will be more strongly held than those bound to $Mn^{3+/4+}$ due to the high crystal field stabilization energy (CFSE) of the low-spin Co^{3+} ion [15]. This would increase the activation energy at these sites, resulting in a slower reaction rate [56]. Secondly, the As(III) oxidation by birnessites is a complex process. Investigation on the arsenite oxidation by a poorly crystalline manganese-oxide exhibited that As(III) oxidation and As(V) sorption is greatly affected by Mn AOS in

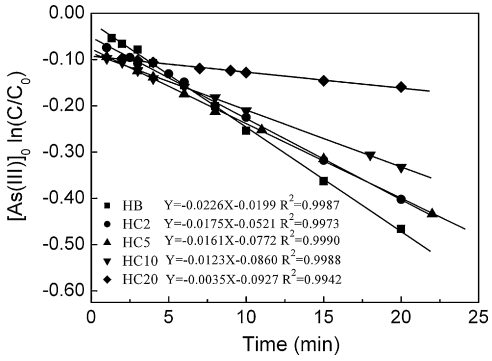

Fig. 9. Linear regression analysis of normalized As(III) uptake by as-obtained birnessite.

the δ-MnO_2 structure [57]. The Mn(III) reactive sites on Mn-oxide surfaces were expected to be less reactive than Mn(IV) reactive sites in terms of As(III) oxidation [39,58,59]. Moreover, analysis of XPS and the release of ions during Pb^{2+} adsorption revealed that certain amounts of $Mn^{2+/3+}$ and $Co^{2+/3+}$ were adsorbed on the surface of birnessites. These low valence ions also blocked reactive sites on the mineral surface.

Release of Mn^{2+}, Co^{2+} and K^+ into the solution was also monitored. The concentrations of K^+ released by HB, HC2, HC5, HC10 and HC20 during the arsenite oxidation process were 1998, 1523, 1247, 1068 and 669 mmol kg^{-1}, respectively. However, Mn^{2+} and Co^{2+} were not detected when HB, HC2, and HC5 were used as oxidants. For HC10 and HC20, 13 and 0, 36 and 8 mmol kg^{-1} of Mn^{2+} and Co^{2+} were determined, respectively. There were two reasons for this low Mn^{2+}/Co^{2+} release: (*i*) MnO_2 particle surface contained negatively charged surface functional groups (≡Mn–O^-), thus soluble $Mn^{2+/3+}$ and $Co^{2+/3+}$ formed by reductive dissolution of Co-containing birnessites were adsorbed on the surface at pH 7.00 in the present study, and (*ii*) the precipitate of $Co_3(AsO_4)_2$ (pK_{sp} = 28.17) [60] and the possible Krautite was formed [61].

The oxidation of As(III) by manganese oxide was an important reaction in both the natural cycling of As and in developing remediation technology for lowering the As(III) concentration in drinking water. In the presence of Co-containing birnessite, As(III) in wastewater or underground water would be oxidized to As(V). As(III) has higher mobility and weaker adsorption, and thereby is more poisonous than As(V) [8]. Because As(V) exists as deprotonated oxyanions in broad pH ranges [23] and has high affinity of mineral surfaces, oxidation of As(III) to As(V) not only reduces its toxicity, but also facilitates the removal of As species. Metal compounds (Fe/Al oxides, hydroxides, etc.) are the most widely used adsorbents for As, for their higher removal efficiency at lower cost versus many other adsorbents [4]. The maximum amount of As(V) produced during the oxidation of As(III) by birnessite was greatly enhanced in the presence of goethite. The combined effects of the oxidation (by birnessite)-adsorption (by goethite) led to rapid oxidation and immobilization of As and alleviation of the As toxicity in the environments [62]. Hence, the powerful oxidation of arsenite by manganese oxides, followed by adsorption of arsenate by Fe/Al compounds as adsorbents, is an applicable approach for the treatment of As(III) contaminated water systems, and is worth further investigation.

4. Conclusions

Co^{2+} ion exchange with birnessite was conducted at different Co^{2+} concentrations. Co^{2+} ions were totally retained by birnessite at low concentrations. However, when initial Co/Mn molar ratio was increased to 0.2, only 80% of Co^{2+} could be located in the structure. Induction of Co^{2+} had no effect on the crystal structure and morphology of birnessite. The crystallinity of Co-containing birnessites gradually decreased and specific surface areas increased. The valence of Co was exclusively +3 and Mn AOS of Co-containing birnessites gradually decreased. The content of hydroxyl groups in the structure of Co-containing birnessites gradually decreased, which accounted for the reduced Pb^{2+} adsorption capacities. As(III) oxidation by Co-containing birnessite was enhanced. Conversely, with an increase in cobalt concentration, the initial reaction rate constant was greatly reduced. During the process of Co^{2+} oxidation, Mn(IV) was more likely the electron sink, and subsequently reduced to Mn(III). The present work provides a new insight into the environmental chemical behavior and interaction mechanism of cobalt and manganese oxides. Further, these modified materials have higher adsorption capacity for Pb^{2+} than many other adsorbents. Simultaneously, their enhanced oxidation ability for As(III) to As(V) can greatly reduce the toxicity of As(III) in the environment. These as-obtained birnessites have great potential applications in the remediation of heavy metal-contaminated soil and water.

Acknowledgements

The authors gratefully thank the National Natural Science Foundation of China (Grant numbers: 40830527, 41171375) and the Fundamental Research Funds for the Central Universities (Program number: 2011PY015) for financial support. The authors also acknowledge research assistant Homer Genuino at University of Connecticut for improving English writing in the paper.

Appendix A. Supplementary data

Supplementary data associated with this article can be found, in the online version, at doi:10.1016/j.jhazmat.2011.09.027.

References

[1] Y.N. Vodyanitskii, Mineralogy and geochemistry of manganese: a review of publications, Eurasian Soil Sci. 42 (2009) 1170–1178.
[2] F. Liu, C. Colombo, P. Adamo, J.Z. He, A. Violante, Trace elements in manganese–iron nodules from a Chinese Alfisol, Soil Sci. Soc. Am. J. 66 (2002) 661–670.
[3] R.P. Han, W.H. Zou, Z.P. Zhang, J. Shi, J.J. Yang, Removal of copper(II) and lead(II) from aqueous solution by manganese oxide coated sand. I. Characterization and kinetic study, J. Hazard. Mater. B137 (2006) 384–395.
[4] D. Mohan, C.U. Pittman Jr., Arsenic removal from water/wastewater using adsorbents—A critical review, J. Hazard. Mater. 142 (2007) 1–53.
[5] X.H. Feng, L.M. Zhai, W.F. Tan, F. Liu, J.Z. He, Adsorption and redox reactions of heavy metals on synthesized Mn oxide minerals, Environ. Pollut. 147 (2007) 366–373.
[6] R.N. Dai, J. Liu, C.Y. Yu, R. Sun, Y.Q. Lan, J.D. Mao, A comparative study of oxidation of Cr(III) in aqueous ions, complex ions and insoluble compounds by manganese-bearing mineral (birnessite), Chemosphere 76 (2009) 536–541.
[7] Y.T Meng, Y.M. Zheng, L.M. Zhang, J.Z. He, Biogenic Mn oxides for effective adsorption of Cd from aquatic environment, Environ. Pollut. 157 (2009) 2577–2583.
[8] X.J. Li, C.S. Liu, F.B. Li, Y.T. Li, L.J. Zhang, C.P. Liu, Y.Z. Zhou, The oxidative transformation of sodium arsenite at the interface of δ-MnO_2 and water, J. Hazard. Mater. 173 (2010) 675–681.
[9] S.B. Lee, J.S. An, Y.J. Kim, K. Nam, Binding strength-associated toxicity reduction by birnessite and hydroxyapatite in Pb and Cd contaminated sediments, J. Hazard. Mater. 186 (2011) 2117–2122.
[10] R.G. Burns, V.M. Burns, The mineralogy and crystal chemistry of deep-sea manganese nodules—a polymetallic resource of the twenty-first century, Philos. Trans. R. Soc. London Ser. A286 (1977) 283–301.
[11] R.M. Taylor, R.M. Mckenzie, The association of trace elements with manganese minerals in Australian soils, Aust. J. Soil Res. 4 (1966) 29–39.
[12] R.M. Mckenzie, The reaction of cobalt with manganese dioxide minerals, Aust. J. Soil Res. 8 (1970) 97–106.
[13] R.M. Mckenzie, The adsorption of lead and other heavy metals on oxides of manganese and iron, Aust. J. Soil Res. 18 (1980) 61–73.
[14] R.G. Burns, The uptake of cobalt into ferromanganese nodules, soils, and synthetic manganese(IV) oxides, Geochim, Cosmochim. Acta 40 (1976) 95–102.

[15] R.G. Burns, Mineralogical Applications of Crystal Field Theory, 2nd ed., Cambridge University Press, Cambridge, 1993.
[16] C.P. Lienemann, M. Taillefert, D. Perret, J.F. Gaillard, Association of cobalt and manganese in aquatic systems: chemical and microscopic evidence, Geochim. Cosmochim. Acta 61 (1997) 1437–1446.
[17] Y. Takahashi, A. Manceau, N. Geoffroy, M.A. Marcus, A. Usui, Chemical and structural control of the partitioning of Co, Ce, and Pb in marine ferromanganese oxides, Geochim. Cosmochim. Acta 71 (2007) 984–1008.
[18] J.W. Murray, J.G. Dillard, The oxidation of cobalt(II) adsorbed on manganese dioxide, Geochim. Cosmochim. Acta 43 (1979) 781–787.
[19] D.L. Crowther, J.G. Dillard, J.W. Murray, The mechanism of Co(II) oxidation on synthetic birnessite, Geochim. Cosmochim. Acta 47 (1983) 1399–1403.
[20] S. Fendorf, P.M. Jardine, R.R. Patterson, D.L. Taylor, S.C. Brooks, Pyrolusite surface transformations measured in real-time during the reactive transport of Co(II)EDTA^{2-}, Geochim. Cosmochim. Acta 63 (1999) 3049–3057.
[21] A. Manceau, V.A. Drits, E. Silvester, C.L. Bartoli, B. Lanson, Structural mechanism of Co^{2+} oxidation by the phyllomanganate buserite, Am. Mineral. 82 (1997) 1150–1175.
[22] S.H. Lee, T.W. Kim, D.H. Park, J.H. Choy, S.J. Hwang, Single-step synthesis, characterization, and application of nanostructured $K_xMn_{1-y}Co_yO_{2-\delta}$ with controllable chemical compositions and crystal structures, Chem. Mater. 19 (2007) 5010–5017.
[23] D.R. Lide, W.M. Mickey Haynes, Handbook of Chemistry and Physics, 19th ed., CRC Press/Taylor and Francis, Florida, 2010.
[24] H. Yin, X.H. Feng, G.H. Qiu, W.F. Tan, F. Liu, Characterization of Co-doped birnessites and application for removal of lead and arsenite, J. Hazard. Mater. 188 (2011) 341–349.
[25] R.M. McKenzie, The synthesis of birnessite, cryptomelane, and some other oxides and hydroxides of manganese, Miner. Mag. 38 (1971) 493–503.
[26] N. Kijima, H. Yasuda, T. Sato, Y. Yoshimura, Preparation and characterization of open tunnel oxide α-MnO_2 precipitated by ozone oxidation, J. Solid State Chem. 159 (2001) 94–102.
[27] D.J. Miller, M.C. Biesinger, N.S. McIntyre, Interactions of CO_2 and CO at fractional atmosphere pressures with iron and iron oxide surfaces: one possible mechanism for surface contamination? Surf. Interface Anal. 33 (2002) 299–305.
[28] M.C. Biesinger, B.P. Payne, A.P. Grosvenor, L.W.M. Lau, A.R. Gerson, R.S.C. Smart, Resolving surface chemical states in XPS analysis of first row transition metals, oxides and hydroxides: Cr, Mn, Fe, Co and Ni, Appl. Surf. Sci. 257 (2011) 2717–2730.
[29] D.W. Oscarson, P.M. Huang, W. Liaw, The oxidation of arsenite by aquatic sediments, J. Environ. Qual. 9 (1980) 700–703.
[30] M. Villalobos, B. Toner, J. Bargar, G. Sposito, Characterization of the manganese oxide produced by *Pseudomonas putida* strain MnB1, Geochim. Cosmochim. Acta 67 (2003) 2649–2662.
[31] M. Villalobos, B. Lanson, A. Manceau, B. Toner, G. Sposito, Structural model for the biogenic Mn oxide produced by *Pseudomonas putida*, Am. Mineral. 91 (2006) 489–502.
[32] J.B. Kim, J.B. Dixon, C.C. Chusuei, Y.J. Deng, Oxidation of chromium(III) to (VI) by manganese oxides, Soil Sci. Soc. Am. J. 66 (2002) 306–315.
[33] R.M. Potter, G.R. Rossman, The tetravalent manganese oxides: identification, hydration, and structural relationships by infrared spectroscopy, Am. Mineral. 64 (1979) 1199–1218.
[34] C.M. Julien, M. Massot, C. Poinsignon, Lattice vibrations of manganese oxides: Part I. Periodic structures, Spectrochim. Acta A: Mol. Biomol. Spectrosc. 60 (2004) 689–700.
[35] A. Chahi, S. Petit, A. Decarreau, Infrared evidence of dioctahedral–trioctahedral site occupancy in palygorskite, Clays Clay Miner. 50 (2002) 306–313.
[36] R.D. Shannon, Revised effective ionic radii and systematic studies of interatomic distances in halides and chalcogenides, Acta Crystallogr. A 32 (1976) 751–767.
[37] J. Portier, G. Campet, J. Etourneau, B. Tanguy, A simple model for the estimation of electronegativities of cations in different electronic states and coordinations, J. Alloys. Compd. 209 (1994) 285–289.
[38] S. Martinez-Alonso, J.R. Rustad, A.F.H. Goetz, Ab initio quantum mechanical modelling of infrared vibrational frequencies of the OH group in dioctahedral phyllosilicates. Part II: main physical factors governing the OH vibrations, Am. Mineral. 87 (2002) 1224–1234.
[39] H.W. Nesbitt, G.W. Canning, G.M. Bancroft, XPS study of reductive dissolution of 7 Å-birnessite by H_3AsO_3, with constraints on reaction mechanism, Geochim. Cosmochim. Acta 62 (1998) 2097–2110.
[40] V.A. Drits, E.J. Silvester, A.I. Gorshkov, A. Manceau, Structure of synthetic monoclinic Na-rich birnessite and hexagonal birnessite: I. Results from X-ray diffraction and selected-area electron diffraction, Am. Mineral. 82 (1997) 946–961.
[41] B. Lanson, V.A. Drits, E.J. Silvester, A. Manceau, Structure of H-exchanged hexagonal birnessite and its mechanism of formation from Na-rich monoclinic buserite at low pH, Am. Mineral. 85 (2000) 826–838.
[42] S.M. Webb, G.J. Dick, J.R. Bargar, B.M. Tebo, Evidence for the presence of Mn(III) intermediates in the bacterial oxidation of Mn(II), Proc. Natl. Acad. Sci. U.S.A. 102 (2005) 5558–5563.
[43] J.J. Morgan, Manganese in natural waters and Earth's crust: its availability to organisms, in: A. Sigel, H. Sigel (Eds.), Metal Ions in Biological Systems, Manganese and its Role in Biological Processes, Marcel Dekker, New York, 2000.
[44] S.W. Knipe, J.R. Mycroft, A.R. Pratt, H.W. Nesbitt, G.M. Bancroft, X-ray photoelectron spectroscopic study of water adsorption on iron sulphide minerals, Geochim. Cosmochim. Acta 59 (1995) 1079–1090.
[45] A.S. Özcan, Ö. Gök, A. Özcan, Adsorption of lead(II) ions onto 8-hydroxy quinoline-immobilized bentonite, J. Hazard. Mater. 161 (2009) 499–509.
[46] S.M. Maliyekkal, K.P. Lisha, T. Pradeep, A novel cellulose-manganese oxide hybrid material by *in situ* soft chemical synthesis and its application for the removal of Pb(II) from water, J. Hazard. Mater. 181 (2010) 986–995.
[47] C.H. Giles, T.H. MacEwan, S.N. Nakhwa, D. Smith, Studies in adsorption. Part XI. A system of classification of solution adsorption isotherms and its use in diagnosis of adsorption mechanisms and in measurement of specific surface area of solids, J. Chem. Soc. 3 (1960) 3973–3993.
[48] D.G. Kinniburgh, General purpose adsorption isotherms, Environ. Sci. Technol. 20 (1986) 895–904.
[49] R.P. Han, W.H. Zou, H.K. Li, Y.H. Li, J. Shi, Copper(II) and lead(II) removal from aqueous solution in fixed-bed columns by manganese oxide coated zeolite, J. Hazard. Mater. B137 (2006) 934–942.
[50] E. Eren, B. Afsin, Y. Onal, Removal of lead ions by acid activated and manganese oxide-coated bentonite, J. Hazard. Mater. 161 (2009) 677–685.
[51] K.D. Kwon, K. Refson, G. Sposito, Surface complexation of Pb(II) by hexagonal birnessite nanoparticles, Geochim. Cosmochim. Acta 74 (2010) 6731–6740.
[52] W. Zhao, Q.Q. Wang, F. Liu, G.H. Qiu, W.F. Tan, X.H. Feng, Pb^{2+} adsorption on birnessite affected by Zn^{2+} and Mn^{2+} pretreatments, J. Soil Sediment. 10 (2010) 870–878.
[53] M. Villalobos, J. Bargar, G. Sposito, Mechanisms of Pb(II) sorption on a biogenic manganese oxide, Environ. Sci. Technol. 39 (2005) 569–576.
[54] M.G. Keizer, W.H. Van Riemsdijk, ECOSAT: Equilibrium Calculation of Speciation and Transport, User Manual Version 4.7, Wageningen Agricultural University, The Netherlands, 1999.
[55] A. Amirbahman, D.B. Kent, G.P. Curtis, J.A. Davis, Kinetics of sorption and abiotic oxidation of arsenic(III) by aquifer materials, Geochim. Cosmochim. Acta 70 (2006) 533–547.
[56] R.M. Mckenzie, The influence of cobalt on the reactivity of manganese dioxide, Aust. J. Soil Res. 9 (1971) 55–58.
[57] B.J. Lafferty, M. Ginder-Vogel, M.Q. Zhu, K.J.T. Livi, D.L. Sparks, Arsenite oxidation by a poorly crystalline manganese-oxide. 2. Results from X-ray absorption spectroscopy and X-ray diffraction, Environ. Sci. Technol. 44 (2010) 8467–8472.
[58] C. Tournassat, L. Charlet, D. Bosbach, A. Manceau, Arsenic(III) oxidation by birnessite and precipitation of manganese(II) arsenate, Environ. Sci. Technol. 36 (2002) 493–500.
[59] M.Q. Zhu, K.W. Paul, J.D. Kubicki, D.L. Sparks, Quantum chemical study of arsenic(III,V) adsorption on Mn-Oxides: implications for arsenic(III) oxidation, Environ. Sci. Technol. 43 (2009) 6655–6661.
[60] J.G. Speight, Lange's Handbook of Chemistry, 16th ed., McGraw-Hill Press, New York, 2005.
[61] B.A. Manning, S.E. Fendorf, B. Bostick, D.L. Suarez, Arsenic(III) oxidation and arsenic(V) adsorption reactions on synthetic birnessite, Environ. Sci. Technol. 36 (2002) 976–981.
[62] X.H. Feng, W.F. Tan, F. Liu, H.D. Ruan, J.Z. He, Oxidation of AsIII by several manganese oxide minerals in absence and presence of goethite, Acta Geol. Sin. (Engl.) 80 (2006) 249–256.